

Fabrication and Characterization of the PMMA/G/Ag Nanocomposite by Pulsed Laser Ablation (PLAL)

Musaab Khudhur Mohammed¹✉, Ghaleb Al-Dahash², Amer Al-Nafiey²✉

¹University of Babylon, College of Education for Pure Sciences, Department of Physics, Hillah, 51001, Iraq.

²University of Babylon, College of Science for Women, Department of Laser Physics, Hillah, 51001, Iraq.

✉ Corresponding authors. E-mail: pure.musaab.kh@uobabylon.edu.iq; amer76z@yahoo.com

Received: Oct. 5, 2021; **Accepted:** Apr. 21, 2022; **Published:** Apr. 21, 2022

Citation: Musaab Khudhur Mohammed, Ghaleb Al-Dahash, and Amer Al-Nafiey, Fabrication and Characterization of the PMMA/G/Ag Nanocomposite by Pulsed Laser Ablation (PLAL). *Nano Biomed. Eng.*, 2022, 14(1): 15-22.

DOI: 10.5101/nbe.v14i1.p15-22.

Abstract

In this work, By using the laser ablation technique (PLAL) to fabricate novel PMMA/G/Ag nanocomposites with less laser energy and short time ablation and study the structural, morphological and optical properties. The X-ray diffraction (XRD) confirmed that the GNPs and AgNPs in the PMMA matrix have a crystallite size increased with increasing the pulse number. Also, the SEM images confirm the homogeneous distribution of the GNPs and AgNPs in the PMMA matrix and the sizes of particles in the nanoscale. Additionally, the link between GNPs and AgNPs in the polymer matrix has been confirmed by the FTIR. Moreover, UV-VIS spectroscopy was studied and confirm the nanocomposite has optical properties with the presence of the polymer as a host and calculating the optical energy gap. For that, this novel nanocomposite with these properties promising for many applications. Finally, the study proved that the PLAL is very suitable for decorated graphene and metal on the polymer matrix with lower pulse laser energy and short ablation time.

Keywords: PLAL, Graphene, Silver, Polymer, Nanocomposite, Characterization, Properties

Introduction

Graphene is a 2D dimensional Hexagonal lattice made up of a single sheet of carbon atoms tightly packed together [1]. Due to its unique electrical, optical, and mechanical properties, graphene is attracting increasing interest from a variety of research fields. It is a zero-band gap semiconductor that is not expected to be photoactive or photo luminescent. Other important features include a high optical transmittance (97.3%) [2-7]. As a result of the discovery of graphene, Geim A. K. and et. al. were awarded the Nobel Prize in Physics in 2010 [8].

Mechanical exfoliation [9], graphite intercalation [10], epitaxial growth of silicon carbide pyrolysis

[11], an electrochemical technique [12], reduction of oxidized graphite [13], and chemical vapor deposition CVD [14] are some of the methods used to make graphene. These techniques, which include multiple steps and the use of strong reducing agents, are not environmentally friendly. On the other hand, pulsed laser ablation in liquid (PLAL) is another method for producing graphene due to its cleanliness, simplicity, ease of particle synthesis at the nanoscale, and strong tools for controlling the final production of the laser ablation process [15-18]. Besides, an important way to purify the particle size produced in this way is to use the newest method as in the [19]. A few polymers can be extended essentially by homogeneously joining graphene due to their low Young's modulus,

making polymer/graphene nanocomposites appealing for a variety of applications. Polymer-graphene nanocomposites, such as poly(methyl methacrylate (PMMA) prepared by a simple casting method [20] and graphene/polyvinyl alcohol (PVA) nanocomposite films, have been fabricated using various techniques such as a facial aqueous solution [21], simple solution method [22], and solution cast method [23]. While many achievements have been made, such as graphene and various metallic nanoparticle like silver (Ag) [24, 25], copper (Cu) [26], and gold (Au) [27]. In this article, we propose a new method for the production of nanocomposites PMMA/G/Ag by PLAL technique with lower pulse laser energy and short ablation time.

Experimental

Preparation of graphite (G) and Silver (Ag) plate

Graphite powder (5 g) and silver powder (5 g) weight (99.99%; Interchemiques SA, Germany) (99.99 percent quality; Sigma Aldrich, St. Louis, MO). After cleaning the cylinder with ethanol, the graphite and silver powders were compressed with a hydraulic piston under pressures of 20 MPa for the graphite powder and 22 MPa for the silver powder, with widths of 2 cm and thicknesses of 2 mm, and then annealed for 4 hours at 450 °C for strengthening. Graphite and silver plate have been cleaned by using cleaned paper and washed with ethanol and refined water to avoid degradation.

Preparation of solvent of poly (methyl methacrylate) (PMMA)

0.5 g Poly(methyl methacrylate) (molecular weight 120000 g/mol, glass temperature 106 °C, density 1.2 /cm³) was dissolved in 30 mL chloroform for 10 minutes with a magnetic stirrer at 40 °C.

Synthesis of PMMA/G/Ag nanocomposite by laser ablation in liquid

The prepared graphite plate was placed on a bracket 2 mm below the liquid surface in a glass vessel filled with 5 mL of the PMMA solution and then exposed with (100, 200, 300, and 400) pulses using a pulsed Q-Switched Nd: YAG laser. As shown in Fig. 1, the pulse has a duration of 10 ns and a repetition rate of 6 Hz at a wavelength of 1064 nm with an energy of 80 mJ per pulse. This colloid solution PMMA/G nanocomposite will be decorated with AgNPs by immersing an Ag plate in this nanocomposite solution and exposing it to

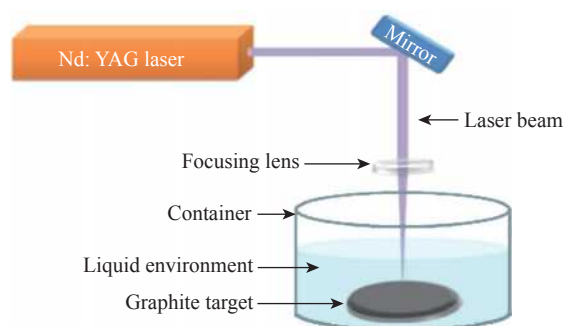


Fig. 1 Laser ablation setup.

(400, 500, 600, and 700) pulses with an energy of 160 mJ from the same Q-Switched Nd: YAG laser, and then preparing the colloid PMMA/G/Ag. By using casting methods on the petri dish to prepare films from this nanocomposite.

By using the dynamic light scattering and interferometric method to find concentration for the GNPs and AgNPs in part per million gram (ppm) in 10ml of the PMMA solvent and thickness for all the films prepared. The concentration of the GNPs and AgNPs and the thickness films increased with increasing the number of pulses as shown in Table 1.

Table 1 The concentration of the GNPs, Ag NPs and thickness for all the prepared films

Symbol	Nanocomposites	Concentrations	Film thickness (μm)
--	PMMA		1.06
S1	PMMA/(G100 p)	G = 20 ppm/10 mL	1.46
S2	PMMA/G(100 p)/ Ag(400 p)	G = 24 ppm/10 mL Ag = 32 ppm/10 mL	1.48
S3	PMMA/G(200 p)/ Ag (500 p)	G = 34 ppm/10 mL Ag = 57 ppm/10 mL	1.66
S4	PMMA/G(300 p)/ Ag(600 p)	G = 77 ppm/10 mL Ag = 83 ppm/10 mL	1.78
S5	PMMA/G(400 p)/ Ag(700 p)	G = 87 ppm/10 mL Ag = 97 ppm/10 mL	1.83

Characterization

To obtain information about the atomic structure of the materials, Philips PW X-ray diffraction technique (XRD-6000-SHIMADZU) with Cu-Kα radiation source at $2\theta = (0-80)$ degree. To investigate the morphology of prepared samples, Hitachi S4160 was used in scanning electron microscopy (SEM). To obtain the structural characterizations of the prepared nanocomposite, FTIR spectroscopy (Shimadzu, IRAffinity-1, Japan) in the 500-4000 cm⁻¹). To investigate the UV-Visible used (Shimadzu UV-1650 PC) made by Phillips, (Japanese company) for the wavelength range from 200 to 900 nm. To record the spectra, samples were in 10 mm

path length quartz cells with reference to correspond solution.

Results and Discussion

XRD pattern for all the films prepared as shown in Figs. 2 and 3. It can be seen that the peaks of pure PMMA around $2\theta = 14.89^\circ$ corresponding to the polymer's crystalline phase pure PMMA [28] and the GNPs around $2\theta = 26.62^\circ$ for film S1 and 26.34° for S2, S3, S4, S5 corresponding to the miller indices (002) which is comparable with literature data (JCDPS 89-7213) [29] confirming the presence of the hexagonal graphene structure. Also from this figure the AgNPs around $2\theta = 35.06^\circ$, 41.63° , 63.25° , and 77.14° corresponding to the miller indices (111), (200), (220) and (311) respectively were assigned to face-centered cubic (JCPDS File No. 89-3722).24) [30]. From XRD

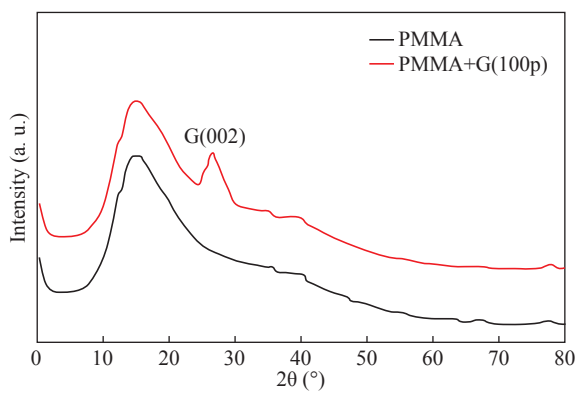


Fig. 2 The XRD spectrum of the pure PMMA and PMMA/G (100 p)

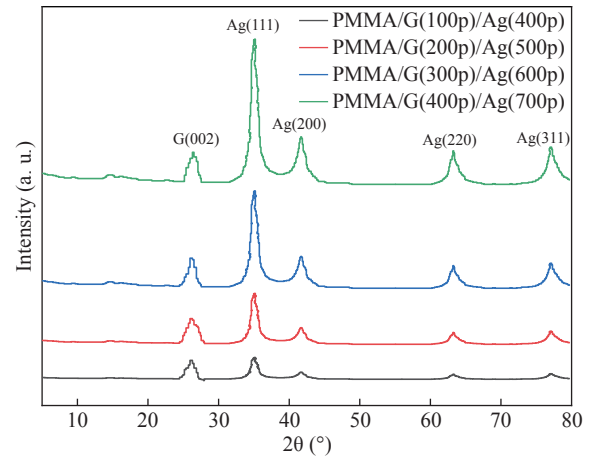


Fig. 3 The spectrum of XRD the PMMA/G/Ag nanocomposite with different pulses number

confirms the presence of the GNPs and AgNPs in the PMMA matrix. The crystallite size has been calculated from Scherer's formula according to the Equation (1) [31]:

$$D = 0, 9\lambda/\beta\cos\theta, \tag{1}$$

where (β) is the full width at the half of the maximum intensity (FWHM) (in radian), (θ) is the Bragg diffraction angle of the XRD peak (degree), and (λ) is the X-ray wavelength (\AA).

It was found that the crystallite size and the intensity of all peaks increased with increasing of the number of pulses. The crystallite size increased from 12.91 nm for film S1 to 27.76 nm for S5. This result is in agreement with the previous studies [20, 32, 33, 34]. The lattice constant a, b and c were calculated by using Equation (2) [31] and listed in Table 2.

Table 2 The XRD results obtained for all the prepared films

Films	2θ	(hkl)	FWHM ($^\circ$)	a (\AA)	b (\AA)	c (\AA)	d (\AA)	Crystallite size (nm)	Average crystallite size (nm)
S1	26.62	G (002)	0.599	2.443	2.436	2.435	3.45	12.91	12.91
	26.34	G (002)	0.477	2.438	1.918	1.917	3.46	16.23	
	35.06	Ag(111)	0.419	2.344	2.344	2.344	2.34	18.09	
S2	41.63	Ag(200)	0.674				2.12	11.03	15.79
	63.25	Ag(220)	0.546				2.22	12.40	
	77.14	Ag(311)	0.405				2.32	15.36	
	26.44	G (002)	0.407	2.439	1.914	1.913	3.47	19.01	
S3	35.12	Ag(111)	0.369	2.355	2.355	2.355	2.33	20.54	18.79
	41.73	Ag(200)	0.474				2.17	15.68	
	63.30	Ag(220)	0.386				2.09	17.55	
	77.28	Ag(311)	0.335				2.18	18.56	
S4	26.54	G (002)	0.377	2.446	1.916	1.917	3.45	20.52	20.45
	35.26	Ag(111)	0.339	2.318	2.318	2.318	2.35	22.35	
	41.86	Ag(200)	0.314				2.26	23.67	
	63.40	Ag(220)	0.346				2.18	19.56	
	77.34	Ag(311)	0.305				2.33	20.38	
S5	26.64	G (002)	0.307	2.438	1.915	1.916	3.44	25.20	27.76
	35.36	Ag(111)	0.289	2.326	2.326	2.326	2.36	26.21	
	41.96	Ag(200)	0.274				2.32	27.12	
	63.44	Ag(220)	0.236				2.35	28.69	
	77.44	Ag(311)	0.205				2.28	30.32	

$$\frac{1}{d^2} = \frac{4}{3} \left(\frac{h^2 + hk + k^2}{a^2} \right) + \frac{l}{c^2} \quad (2)$$

The surface morphology for all the prepared films of the nanocomposite could be observed by the SEM. Figure 4 explain SEM images for all the sample preparation, it is observed that the pure PMMA was homogenous and smooth this indicates a good method for prepared sample, also it is observed that the homogeneous dispersed of GNPs and AgNPs inside PMMA matrix respectively, primarily due to strong covalent interaction between the GNPs and AgNPs in the PMMA matrix [35] determined from FTIR analysis. However, from Table 3, we note that the average particle size increased with increasing of the number of pulses, it is increased from 25 nm to 65 nm in the PMMA matrix. This result attributed to the increasing concentration of the GNPs and AgNPs that was confinement by the dynamic light scattering and

Table 3 The average particle size for all samples obtained from SEM results

Films	Average particle size (nm)
S1	32
S2	54
S3	66
S4	71
S5	95

agreement with XRD spectra, which is importantly used in piezoelectric sensor and optoelectronic detector. This result agrees with the previous studies [20, 34].

The data about the compound holding in the newly created nanomaterials was shown using Fourier transform infrared (FTIR) spectroscopy. Figures 5 and 6 shows FTIR for the graphite powder and PMMA/G/Ag nanocomposite with the different number pulses at room temperature. In the graphite powder spectra, the peaks at (601, 832, 1086, 1240, 1372, 1713, 2911 and 3295) cm^{-1} clearly corresponds to various functionalities including represents bending of C–H, C–C stretching, C–O stretching, C–OH stretching,

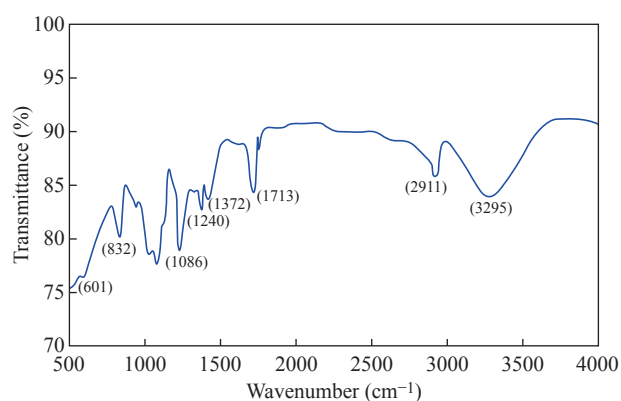


Fig. 5 FTIR spectrum of the graphite powder

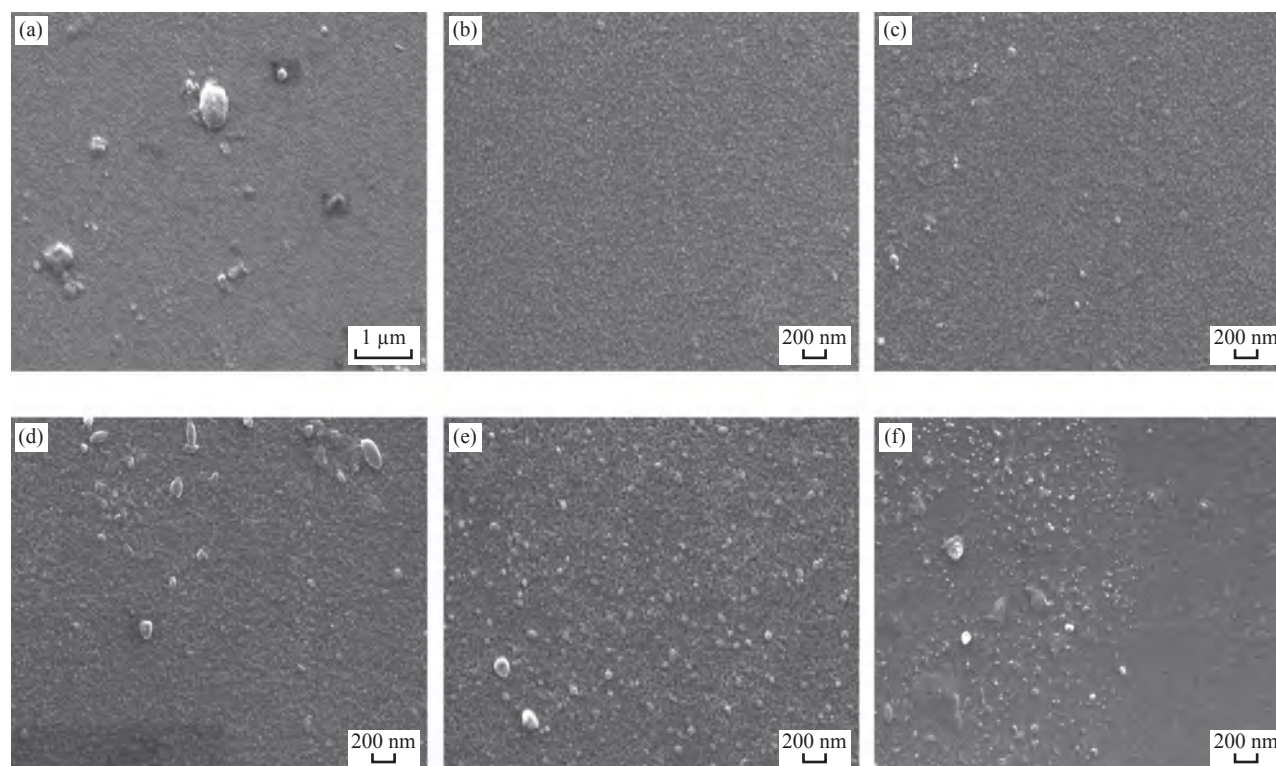


Fig. 4 SEM images for the (a) PMMA, (b) S1, (c) S2, (d) S3, (e) S4 and (f) S5

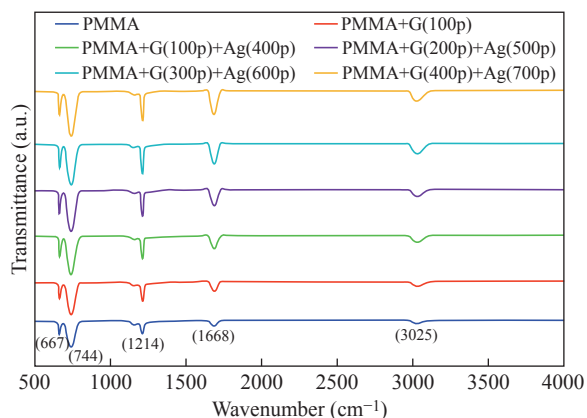


Fig. 6 FTIR spectrum for the PMMA, PMMA/G(100 p) and PMMA/G/Ag nanocomposite with different laser pulses number

plane OH bending mode of hydroxyl groups, C=O stretching and O–H stretching vibration respectively observed [36, 37].

On the other hand, Figure 5 shows the FTIR spectra of the PMMA/G/Ag nanocomposite and pure PMMA, the peaks (667) cm⁻¹ that has been shifted to the higher wavenumber while the peaks (744, 1214, 3025) cm⁻¹ that has been shifted to the lower wavenumber and the peaks (1372, 1086, 1713, 2911) cm⁻¹ of the graphite spectra that disappeared in the PMMA/G/Ag nanocomposite and pure PMMA. A new peak has been observed at (1668) cm⁻¹ due to C=C stretching [38, 39] for the PMMA/G/Ag nanocomposite and pure PMMA that was preferred for the graphene. As a result of the shift to the higher wavenumber side, the molecule's mass is reduced. Because the mass of a vibrating molecule is inversely proportional to its frequency of vibration. As a result, the lighter the molecule, the higher the vibration frequency and wave number. It is noted that the intensity of these peaks is increasing with the increasing of the number of the pulses that was attributed to the increasing of the concentration of the GNPs and AgNPs in the PMMA matrix that was confirmed by the dynamic light scattering and also due to indicating that C=O has been established. This result is in agreement with the previous studies [40].

Strong contact between the GNPs and AgNPs in the PMMA matrix confirmed good interfacial adhesion, which is an important criterion for the nanocomposite to be used as the piezoelectric sensor and optoelectronic detector.

The absorption spectra as a function of the wavelength as shown in Fig. 7. This figure obtains that the absorption increased with increasing of the number pulses laser for all the films prepared, this result due

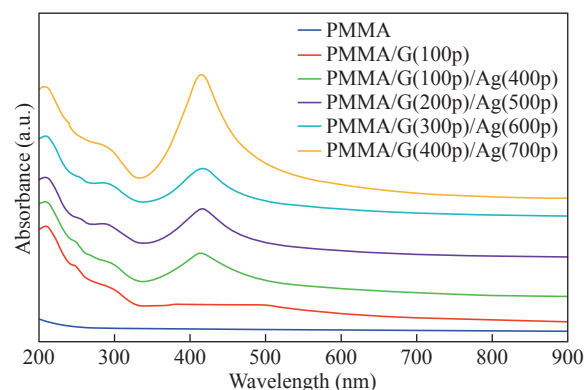


Fig. 7 The absorption spectra of the pure PMMA, and PMMA/G/Ag nanocomposite with different pulses

to increase the concentration of the graphene and silver nanoparticle (GNPs, AgNPs) with increasing the number of the pulses laser was confirmed by the dynamic light scattering. Also, the figures show that the absorption peaks at 280nm in all the films of PMMA solvent. The absorption peak due to π - π^* transition of C=C band and n - π^* transition of C=O band have occurred around 280 nm of the GNPs. These absorption peaks are observed due to Surface Plasmon Resonance (SPR) in the free electron cloud of carbonaceous material π electrons. These absorption peaks a characteristic feature of graphene. This result agrees with the previous studies [41, 42, 43]. While the presence of AgNPs in the nanocomposite was confirmed by the absorption peak at 408nm for the PMMA solvent. This specific range shows the surface Plasmon effect of AgNPs. This confirms the formation and presence of AgNPs in the nanocomposite, due to the SPR of the AgNPs, which is similar to previous studies [32]. Also the main absorption peaks of the GNPs and AgNPs in PMMA solvent shift toward a longer wavelength (redshift) which is different from the position of the main peak of the GNPs and AgNPs in PMMA solvent that indicates the increased particle size and vice versa [44] which is confirmed by the (XRDM SEM and FTIR).

By using Equation (3) to calculate the optical energy gap (E_g) for all the samples prepared [45]:

$$\alpha h\nu = (h\nu - E_g)^r \quad (3)$$

Figs. 8 and 9 show that the indirect optical energy gap for the allowed and forbidden transition electrons respectively for all the films prepared. To determine the (E_g) is to scheme a chart between $(\alpha h\nu)^r$ and photon energy ($h\nu$) and where r is (1/2) or (1/3) for the allowed and forbidden indirect electron transition. Extrapolating the straight pieces of these relations to the $h\nu$ axis

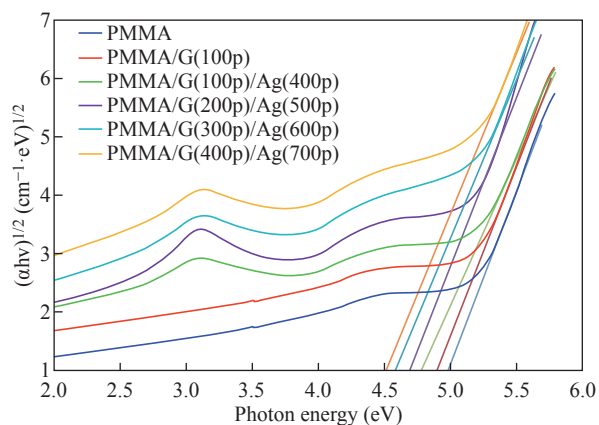


Fig. 8 A plots of $(\alpha hv)^{1/2}$ versus photon energy ($h\nu$) of pure PMMA, PMMA/G(100 p) and PMMA/G/Ag nanocomposite with different pulses

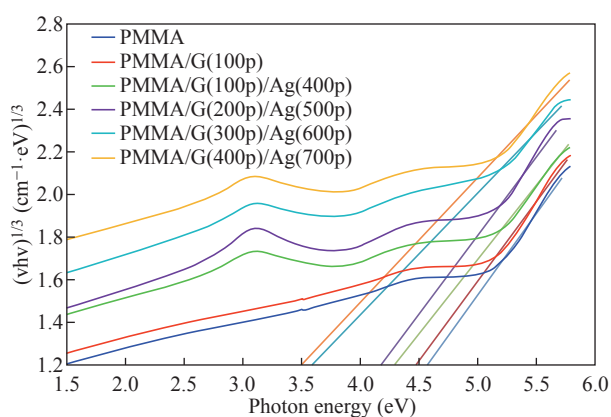


Fig. 9 A plots of $(\alpha hv)^{1/3}$ versus photon energy ($h\nu$) of pure PMMA, PMMA/G(100 p) and PMMA/G/Ag nanocomposite with different pulses

yields the optical band hole estimations which are recorded in a Table 4. From the figures, we note that the E_g decreased from 4.9 to 4.1 eV and 4.55 to 3.5 eV of the allowed and forbidden indirect energy gap with the increasing of the number of the pulses laser for the GNPs and AgNPs for the PMMA solvent. This result is attributed to the increasing concentration of the GNPs and Ag NPS that was proved by the dynamic light scattering. This result due to localized states of the various color centers may lead to a widening of the mobility gap. This overlap may prove to be a reduction

Table 4 The value of allowed and forbidden indirect energy gap for all samples prepared

Films	Allowed E_g (eV)	Forbidden E_g (eV)
PMMA	5	4.6
S1	4.9	4.5
S2	4.8	4.3
S3	4.7	4.2
S4	4.6	3.6
S5	4.5	3.5

in the energy gap when the concentration of GNPs and AgNPs in the PMMA solvent increases. This result agrees with the previous studies [46].

Conclusions

In summary, the PLAL technique has been employed to manufacture PMMA/G/Ag nanocomposites for using less laser energy and short time ablation. The presence in the PMMA matrix of GNPs and AgNPs was confirmed by XRD and the crystallite size was increased as the number of pulses increased. In SEM images, the GNPs and AgNPs are shown in the PMMA matrix as a homogeneous distribution. The link between polymer network and GNPs, AgNPs have been shown by FTIR to be sufficient to have stable nanocomposite. Also studied was UV-VIS spectroscopy. In the PMMA solvent, the absorption peak for GNPs at 280 nm and for AgNPs at 408 nm, and all nanocomposite have an indirect optical energy gap for the allowed and forbidden transition electron and with increasing concentration of GNPs and AgNPs in nanocomposite, the optical energy gap decreased for the allowed and forbidden transition electron. We have demonstrated a new method for producing and synthesizing such polymeric composites using laser ablation.

References

- [1] K.S. Novoselov, A.K. Geim, S.V. Morozov, D. Jiang, M.I. Katsnelson, I.V. Grigorieva, S.V. Dubonos, A.A. Firsov, Two-dimensional gas of massless Dirac fermions in graphene, *Nature*, 438, 2005, 197-200.
- [2] A.K. Geim, K.S. Novoselov, The rise of graphene, *Nat. Mater.* 6, 2007, 183-191.
- [3] A.C. Ferrari, D.M. Basko, Raman spectroscopy as a versatile tool for studying the properties of graphene, *Nat. Nanotechnol.* 8, 2013, 235-246.
- [4] R. Sahin, E. Simsek, S. Akturk, Nanoscale patterning of graphene through femtosecond laser ablation, *Appl. Phys. Lett.* 104, 2014, 053118.
- [5] Xian-Fu. Zhang, Xiaona. Shao, Suping Liu, Dual Fluorescence of Graphene Oxide: A Time-Resolved Study, *J. Phys. Chem. A* 116, 2012, 7308-7313.
- [6] A. Tiwari, Syväjärvi M. Graphene Materials: Fundamentals and Emerging Applications. *John Wiley & Sons*, 2015
- [7] Novoselov, K.S. Nobel lecture: Graphene: Materials in the flatland. *Reviews of Modern Physics*, 83, 837, 2011
- [8] J. Wei, Atif R., Vo T and Inam F. Graphene nanoplatelets in epoxy system: dispersion, reaggregation, and mechanical properties of nanocomposites. *J. of Nanomaterials* 16, 374, 2015
- [9] Musaab Khudhur Mohammed, Amer Al-Nafiey, and Ghaleb Al-Dahash. Manufacturing Graphene and Graphene-based Nanocomposite for Piezoelectric Pressure Sensor Application: A Review. *Nano Biomed.*

- Eng 13. 1, 2021, 27-35.
- [10] X. Li, Zhang G., Bai X., Sun X., Wang X., Wang E. and Dai H.. Highly conducting graphene sheets and Langmuir-Blodgett films, *Nat. Nanotechnol.*, 3, 538, 2008
- [11] M.L. Sadowski, Martinez G., Potemski M., Berger C. and de Heer W.A. Landau Level Spectroscopy of Ultrathin Graphite Layers. *Phys. Rev. Lett.*, 97, 2006, 405.
- [12] N. Liu., Fang L., Haoxi W., Yinghui L., Chao Z., Ji C. One-Step Ionic-Liquid-Assisted Electrochemical Synthesis of Ionic-Liquid-Functionalized Graphene Sheets Directly from Graphite. *Adv. Funct. Mater.*, 18, 2008, 1518.
- [13] Jabir, Majid S., et al. Fe₃O₄ nanoparticles capped with PEG induce apoptosis in breast cancer AMJ13 cells via mitochondrial damage and reduction of NF-κB translocation. *Journal of Inorganic and Organometallic Polymers and Materials*, 31.3 (2021): 1241-1259.
- [14] Khashan, Khawla S., Ghassan M. Sulaiman, and Sura A. Hussain. Synthesis and Characterization of Aluminum Doped Zinc Oxide Nanostructures by Nd: YAG Laser in Liquid. *Iraqi Journal of Science*, 2590-2598, 2020.
- [15] Mostafa, Ayman M., et al. Synthesis of multi-walled carbon nanotubes decorated with silver metallic nanoparticles as a catalytic degradable material via pulsed laser ablation in liquid media. *Colloids and Surfaces A: Physicochemical and Engineering Aspects*, 2021: 126992.
- [16] Mostafa, Ayman M., and Eman A. Mwafy. The effect of laser fluence for enhancing the antibacterial activity of NiO nanoparticles by pulsed laser ablation in liquid media. *Environmental Nanotechnology, Monitoring & Management*, 14 (2020): 100382.
- [17] Bahjat, Hasan H., Raid A. Ismail, and Ghassan M. Sulaiman. Photodetection properties of populated Fe₃O₄@TiO₂ core-shell/Si heterojunction prepared by laser ablation in water. *Applied Physics A*, 128.1, 1-9, 2022.
- [18] Nagham Mohammed, Ghaleb AL-Dahash, Rafee Tuema, A Simple New Method for Purifying Grain Size by Pulse Laser Ablation. *Neuro Quantology*, 18, 2020, 32-36.
- [19] Hussien, Mai S.A., M.I. Mohammed, and I.S. Yahia. Multifunctional applications of graphene-doped PMMA nanocomposite membranes for environmental photocatalytic. *Journal of Inorganic and Organometallic Polymers and Materials*, 2020, 1-12.
- [20] B. Chenlu, Yuqiang G., Lei S., and Yuan H. Poly(vinyl alcohol) nanocomposites based on graphene and graphite oxide: A comparative investigation of property and mechanism. *J. of Materials Chemistry*, 21, 2011, 13942-13950.
- [21] Abu Hannifa A., Zulhelmi I., Anis S.Z.A., Fadwa S.I. and Kamal Y. PVA/Graphene Nanocomposite: Morphology and its Thermal Properties. *IOP Conf. Series: Materials Science and Engineering*, 319, 2018.
- [22] Yanyan F., Ningning D., Gaozhong W., Yuanxin L., Saifeng Z., Kangpeng W., Long Z., Werner J.B. and Jun W. Saturable absorption behavior of free-standing graphene polymer composite films over broad wavelength and time ranges. *Optics Express*, 23, 2015, 559-569.
- [23] Anamt M.N., Muhammad M.S., Perumal R. and Nay M.H. A glassy carbon electrode modified with graphene oxide and silver nanoparticles for amperometric determination of hydrogen peroxide. *J. of Springer*, 2016, 183, 911-916.
- [24] Musaab Khudhur Mohammed, Ghaleb Al-Dahash, and Amer Al-Nafey. Synthesis and characterization of PVA-Graphene-Ag nanocomposite by using laser ablation technique. *Journal of Physics: Conference Series*, 1591, 2020.
- [25] H. Ke-Jing, Lan W., Jing L., Tian G. and Yan-Ming L. Glassy carbon electrode modified with glucose oxidase-graphene-nano-copper composite film for glucose sensing. *Science direct*, 46, 2013, 378-383.
- [26] G. Chang-Jie, Fen-Ying K, Zhi-Dong C., Da-He F., Hai-Lin F. and Wei W. Reduced graphene oxide-Hemin-Au nanohybrids: Facile one-pot synthesis and enhanced electro catalytic activity towards the reduction of hydrogen peroxide. *Biosensors and Bioelectronics*, 78, 2016, 300-307.
- [27] Aziz, Shujahadeen B., Omed Gh Abdullah, Sarkawt A. Hussein, and Hameed M. Ahmed. Effect of PVA blending on structural and ion transport properties of CS: AgNt-based polymer electrolyte membrane. *Polymers*, 9, 2017, 622.
- [28] T.P. Teng, W.P. Wang, Y.C. Hsu, Fabrication and Characterization of Nanocarbon-Based Nanofluids by Using an Oxygen-Acetylene Flame Synthesis System, *Nanoscale Res. Lett.*, 11, 2016.
- [29] Navaladian, S., Viswanathan, B., Varadarajan, T.K., & Viswanath, R.P. Fabrication of worm-like nanorods and ultrafine nanospheres of silver via solid-state photochemical decomposition. *Nanoscale Research Letters*, 4, 2009, 471-479.
- [30] C. Gumus, O. M. Ozkendir, H. Kavak, and Y. Ufuktepe, Structural and optical properties of zinc oxide thin films prepared by spray pyrolysis method. *J. Optoelectronics and Advanced Materials*, 8, 2006, 299-303.
- [31] Singho, Noorsaiyyidah Darman, Mohd Rafie Johan, and Nurul Akmal Che Lah. Temperature-dependent properties of silver-poly(methylmethacrylate) nanocomposites synthesized by in-situ technique. *Nanoscale Research Letters*, 9, 2014, 1-6.
- [32] Khan, Mohammad Ehtisham, Mohammad Mansoob Khan, and Moo Hwan Cho. Biogenic synthesis of a Ag-graphene nanocomposite with efficient photocatalytic degradation, electrical conductivity and photoelectrochemical performance. *New Journal of Chemistry*, 39, 2015, 8121-8129
- [33] Petreska, Gordana Siljanovska, Jadranka Blazevska-Gilev, Radek Fajgar, and Radmila Tomovska. Surface-Enhanced Raman Scattering activity of Ag/graphene/polymer nanocomposite films synthesized by laser ablation. *Thin Solid Films*, 564, 2014, 115-120.
- [34] Ali, Salam H., and Zahraa G. Naji. Structure Properties of Graphene-polymer Nanocomposite. *Engineering and Technology Journal*, 34, 2016.
- [35] B. Adhikari, A. Biswas, A. Banerjee, Graphene oxide-based hydrogels to make metal nanoparticle-containing reduced graphene oxide-based functional hybrid hydrogels, *ACS Appl. Mater. Interfaces*, 4, 2012, 5472-5482.
- [36] C. Hou, Q. Zhang, Y. Li, H. Wang, Graphene-polymer hydrogels with stimulus-sensitive volume changes, *Carbon*, 50, 2012, 1959-1965
- [37] Z. Matusinovic, Rogosic, M.; Sipusic, J. Synthesis and characterization of poly(styrene-comethyl methacrylate)/layered double hydroxide nanocomposites via in situ polymerization. *Polym. Degrad. Stabil.* 94, 2009, 95-101.
- [38] G.N. Vijayakumari, Selvakumar, K. Jeyasubramanian, and R. Mala. Investigation on the Electrical Properties of Polymer metal Nanocomposites for Physiological sensing applications. *Physics Procedia*, 49, 2013, 67-78.
- [39] Aldosari, Mohammad A., Ali A. Othman, and Edreese H. Alsharaeh. Synthesis and characterization of the in situ bulk polymerization of PMMA containing graphene sheets using microwave irradiation. *Molecules*, 18, 2013, 3152-3167.
- [40] Ghavidel, Elham, Amir Hossein Sari, and Davoud Dorrani. Experimental investigation of the effects of different liquid environments on the graphene oxide produced by laser ablation method. *Optics & Laser Technology*, 103, 2018, 155-162.
- [41] M.N. Nnabuchi, ptical and solid state characterization

- of optimized manganese sulphide thin films and their possible applications in solar energy. *The Pacific Journal of Science and Technology*, 7, 2006, 69-76.
- [42] Surudžić, Rade, Ana Janković, Nataša Bibić, Maja Vukašinović-Sekulić, Aleksandra Perić-Grujić, Vesna Mišković-Stanković, Soo Jin Park, and Kyong Yop Rhee. Physico-chemical and mechanical properties and antibacterial activity of silver/poly(vinyl alcohol)/graphene nanocomposites obtained by electrochemical method. *Composites Part B: Engineering*, 85, 2016, 102-112.
- [43] Singho, Noorsaiyyidah Darman, Mohd Rafie Johan, and Nurul Akmal Che Lah. Temperature-dependent properties of silver-poly (methylmethacrylate) nanocomposites synthesized by in-situ technique. *Nanoscale Research Letters*, 9, 2014, 1-6.
- [44] H. Ghanbari, Sarraf-Mamoory R., Sabbaghzadeh J., Chehrghani A. and Malekfar R. Nonlinear optical absorption of carbon nanostructures synthesized by laser ablation of highly oriented pyrolytic graphite in organic solvents. *Int. J. Opt. Photonics*, 7, 2013, 113-124.
- [45] Mehmood, Ahsan, N.M. Mubarak, Mohammad Khalid, Priyanka Jagadish, Rashmi Walvekar, and E.C. Abdullah. Graphene/PVA buckypaper for strain sensing application. *Scientific Reports*, 10, 2020, 1-14.
- [46] H.M. Zidan, M. Abu-Elnader. Structural and optical properties of pure PMMA and metal chloride-doped PMMA films. *Physica B: Condensed Matter*, 355, 2005, 308-317.

Copyright© Musaab Khudhur Mohammed, Ghaleb Al-Dahash, and Amer Al-Naficy. This is an open-access article distributed under the terms of the Creative Commons Attribution License, which permits unrestricted use, distribution, and reproduction in any medium, provided the original author and source are credited.